High Precision 3D LiDAR Signal Processing and System for Multi-User

Kai-jiun Yang, Chi-Tien Sun

***Abstract*—The LiDAR system uses laser pulses to delineate the 3D depth map. The laser pulses are emitted through multiple laser guns with corresponding photo diodes, and the mechanical devices are required so that the detection plane can be wide enough. All these factors make the LiDAR system big and expensive. Additionally, if there are multiple LiDAR systems in the same filed and are detecting at the same time, the measurement can be interfered by one another. In this paper we proposed the algorithm to differentiate different LiDAR systems in the same field and refine the estimation. Moreover, an FPGA platform was built to validate the proposed architecture. The dimension of the platform is greatly reduced and can be applied to portable LiDAR systems. With the proposed modulation scheme, the detecting laser waveform shall not interfere one anther while refining the estimation.**

***Index Terms*—LiDAR, ToF, Curve Fitting, EM Algorithm, Multi-user, Fast Fourier Transform, Time Delay and Phase Rotate Conversion.**

I. Introduction

THE modern real-time object detection uses the methods such as radar, infrared, sonar, night vision, and LiDAR (Light Detection And Ranging). These approaches have various physical limitations and the cost concerns. The detecting range of radar is hundreds of meters, and the detection is based on single point scanning. It only can tell whether the object exists within the effective range. The provided result cannot fully depict the contour of the objects, and the horizontal resolution is less desirable. The costs of infrared and sonar are low, but the effective ranges are within few tens of meters. The resolution is poor and the contour or the objects cannot be fully illustrated as well. The night vision technology captures the image in dark environment through amplifying the dimly reflected light. Its effective range is within hundreds of meters, and the acquired images are in two- dimension without depth information. All of the above techniques are susceptible to the ambient lights, the surrounding climates, or the semi-blockage such as foliage or vapor.

LiDAR uses laser impulses which are highly penetrative and long ranging. The depth map can be acquired through analyzing the timing, the amplitude, and the width of the received pulses. Additionally the generated depth map includes layer information which is selective so that the underneath contour can be told. Moreover, the effective range can be above hundreds of meters depending on the laser type. However, the dimension of the LiDAR system is bulky and expensive, and the calibration is needed for high precision measurement.

As the progress of development in self-driving cars, the features of long-range and the precision in LiDAR are applied for the navigation. The self-driving cars developed by Google have applied the LiDAR system designed by Velodyne as shown in Fig.1 [1]. In the actual piloting scenarios, the LiDAR system needs to counteract the interferences caused by the weather or all kinds of blockage. Another important issue is the interference caused by the other LiDAR systems in the same field. The LiDAR systems actively generate the laser impulses, which can be regarded as the interference when the other LiDAR systems pick up the detecting signals. Therefore, the signal differentiation and encryption also play important roles in the design of LiDAR system.

The analysis of the LiDAR system can be classified into five categories: the laser signal sources, the laser modulation techniques, the detection of the laser signals, the estimation of the distance, and the reconstruction of the depth map. This paper reviews the fundamentals of the LiDAR system and focuses on laser modulation techniques and the estimation of the distance. The algorithms are proposed to suppress those non-ideal interference, which refines the estimation in the frequency domain and compensates the results in time domain. Also an FPGA prototype was built to verify the feasibility and the performance. The results can be applied to portable LiDAR system which are used in self-driving vehicles or artifical visual enhancement.

II. Fundamentals of LiDAR and the Applications

A. Fundamentals

The LiDAR system uses high density laser signals to scan the field and generate 3D depth map based on those reflected laser pulses. Since the laser is a kind of non-dispersive light which can also penetrate water or gaseous medium, it is suitable for all kinds of contactless ranging. Based on the types of the carriers, there are three kinds of LiDAR system: airborne LiDAR, bathymetric LiDAR, and terrestrial LiDAR. Since the LiDAR system uses active light source, it is less susceptible to ambient interference, such that the generated depth map is far more accurate than the one converted from 2D images which can also be compromised by the angles during photographing. According to the forms of the laser signals, there are two kinds of detection used in LiDAR systems: Tof and phase detection.

B. Time of Flight (ToF) Detection

The ToF LiDAR estimates the distance based on the elapsed time that the receiver captures the transmitted pulses [2]. Currently this is the major method used in long range scanning LiDAR. At the transmitter, the laser gun emits the pulses that are of high instantaneous power within the width less than one nano second as shown in Fig.2. The laser pulse travels through the medium and bounces back when hitting impenetrable objects. The target distance can be estimated by calculating the time t that the pulses have traveled

$$R = C \times t / 2 \,. \qquad (1)$$

C is the speed of the light and it is 3×10^8 meters per second. This means that one nano second time difference is 15cm apart. Therefore, one of the import key factors in ToF estimation is the resolution of the receiver in time.

Fig. 1. The self-driving car developed by Google and the LiDAR device HDL-64E designed by Velodyne. The price of the LiDAR device is USD 75,000. [1]

The reflected laser pulses carry additional information other than the distance. Based on the amplitude and the width of the return pulses, the material of the targets can also be told as shown in Fig.2. The larger the intensity in pulse, the harder the object. For example, the intensity shall be different between the pulses that hit the steel and those hit the mud. On the other hand, the width of the pulses can tell whether the surface is tilted.

The crucial feature that makes LiDAR unique is selectable layer rendering. As mentioned earlier, the received time, the pulse width, and the intensity can be interpreted to specific physical characteristics. Therefore, the users can choose the representation based on the features, for example, the reflectivity, of the objects. Additionally, the laser pulses can penetrate multiple layers of certain objects as shown in Fig.2. The single laser pulse not only bounced back when hitting the ground. On its way back, the laser pulse also sweeps through several branches and generates additional small pulses. Hence, the reconstructed depth map of the branches can be selected independently. However, when the resolution of the receiver is low, these multiple pulses can be blur especially when they are close. In this case, the precision of the depth map shall be compromised.

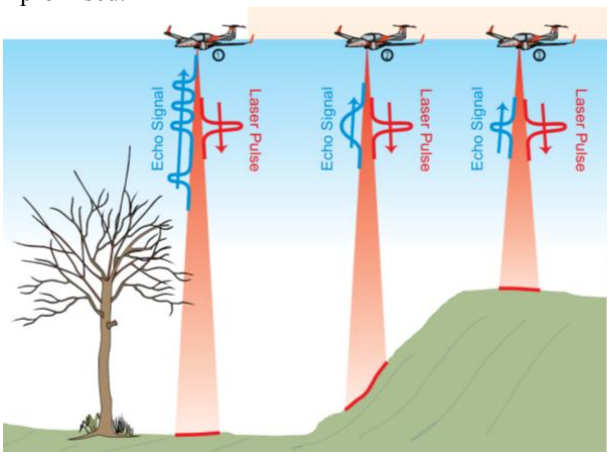

Fig. 2. The principle of ToF LiDAR.

Figure 3 is the depth map of ITRI campus that is captured by airborne LiDAR [3]. Based on the intensity as shown in Fig.3(a), the picture shows the contour of the buildings, the roads, and the bushes. If the received time of the pulses is applied as shown in Fig.3(b), the altitudes of the buildings and the terrain can be perceived.

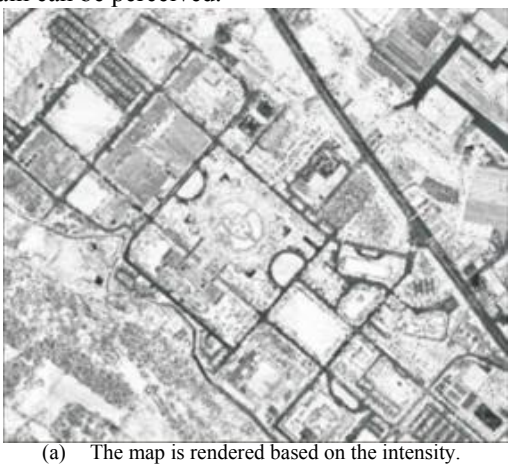

(a) The map is rendered based on the intensity.

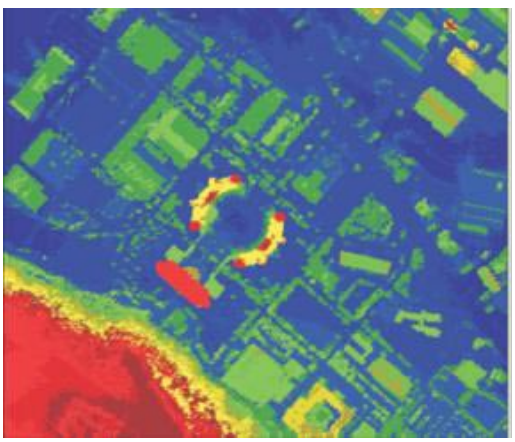

(b) The map is rendered based on the altitude.

Fig. 3. The aerial view of ITRI campus captured by LiDAR. [3]

C. Phase Detection

The phase detection uses the laser emitter that generates long period of continuous laser wave with wavelength λ as illustrated in Fig.4 [4]. By capturing the relevant amplitude of the reflected laser wave, the receiver can tell the phase delay of the emitted detecting laser wave by the delayed wavelength Δ_λ. The estimated distance is derived by

$$R = (M\lambda + \Delta_\lambda)/2 \qquad (2)$$

where M is the number of the periodic laser wave. If the distance to be measured is longer than the wavelength of the periodic laser wave, a timing mark should be added into the laser wave and it is logged at the receiver.

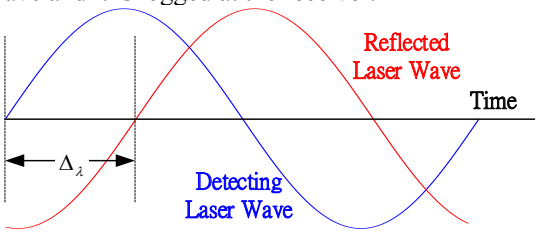

Fig. 4. The principle of phase detection used in LiDAR.

The distance estimation that uses phase detection usually is applied in short range measurement within 100 meters. Due to the power limitation the laser emitter cannot generate periodic laser wave with high energy. However, such a device can be made in compact size and the precision is within centimeters. Figure 5 records the periodic laser wave that is generated by the hand-held laser range finder Bosch GLM80. The spikes are used as timing mark. By accumulating the logged waveform as shown in blue wave for removing the noise, the center frequency is around 2MHz. This means the wavelength is at 150 meters.

During the measurement with the laser range finder, if there's other laser source with the same laser frequency superimposed on the same target, the result shall be erroneous or the measurement fails due to such an interference.

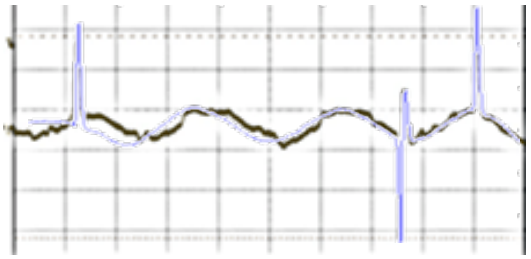

Fig. 5. The logged waveform of the laser waveform generated by Bosch GLM80. The blue wave is the accumulation from 20 logged waveforms.

D. Generation of 2D Detection Matrix

The 2D detection matrix is generated by one or more laser emitters with corresponding photo diodes and the mechanical module for movement control. In Velodyne HDL-64E, there are 64 laser emitters with the sensors, and there's a servomotor that spins in 360 degree to capture the panorama. The updating rate is 5 to 15 times per second. Due to the limitation in mechanical structure, the size is large and the frame rate is restricted. Moreover, such an equipment contains a lot of optical modules and the price can be three times of a compact car.

MEMs mirror steers the reflective surface in 1-D or 2-D, and the round-trip frequency can be as high as thousands of hertz. Initially it was applied in portable projector for the needs of low cost and low power consumption [5]. Single experimental module costs around 10,000 NTD, and the frame rate can be close to hundreds of frames per second. On the other hand, the reflecting angle is within $\pm 15° \sim 20°$, and the module is fragile if there's dust falling on the mirror. Figure 6 shows the laser detcting matrix expanded by the MEMs mirror. The laser emitter generates the laser dot, and the MEMs mirror reflects the dot to the pixel in the frame.

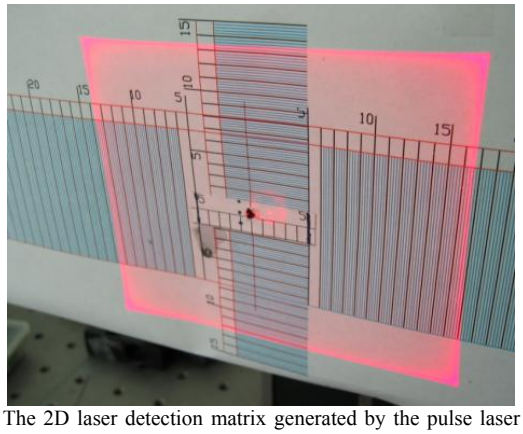

Fig. 6. The 2D laser detection matrix generated by the pulse laser and the MEMs mirror. [5]

E. Terrain Detection

The development of LiDAR system can be dated back to 1980 when NASA initiated the terrain survey. The lasers with different wavelength are of different kinds of penetration. Some can travel though the water while others can go through the bushes. Figure 7 shows the scanning results generated by the LiDAR systems [6]. At the surface layer the distribution of the plants is recorded as shown in Fig.7(a). The pulses that hit the foliage are presented in scattering pattern. If these dots are removed and only the bottom layers are preserved, the topography that is beneath the jungle is surfaced. As mentioned in the earlier paragraph, different combinations of the pulse parameters can highlight certain physical characteristics.

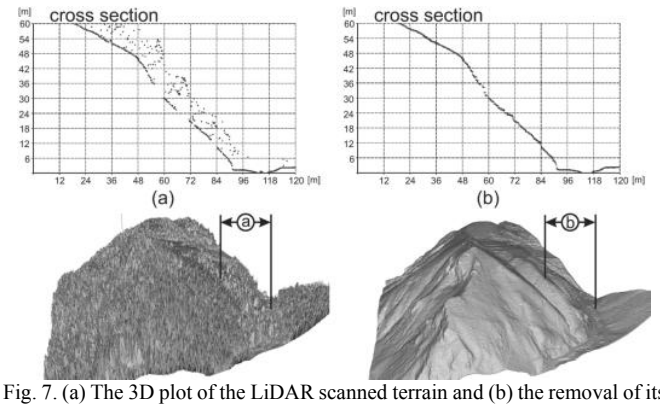

Fig. 7. (a) The 3D plot of the LiDAR scanned terrain and (b) the removal of its vegetation on the slope. [6]

F. *Pilot for Self-Driving*

In order to make the LiDAR system portable and to increase the frame rate, the photo censors along with the DSP blocks were proposed to be integrated into a SoC. Besides using the MEMs mirror to generate the detecting matrix [7], a rotating six prism can generate similar matrix with better robustness [8]. Figure 8 shows the dimension of the prototype, the SoC of the computing core, and the depth map captured in the field. With the features such as active light source and the capability to select the presenting depth, the mobile LiDAR system can effectively suppress the driving interference such as darkness, rain or fogs, and the detection of the obstacles in the driveway can be applied to the navigation.

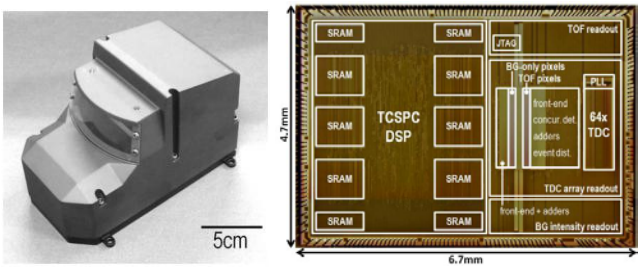

(a) The prototype of the portable LiDAR system with its SoC.

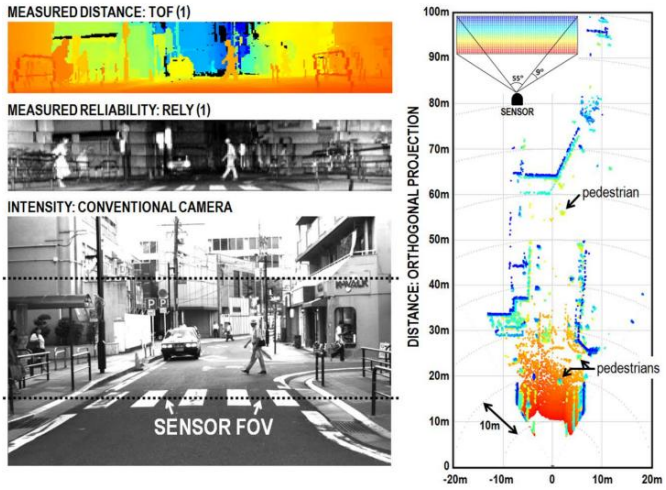

(b) The depth map generated by the prototype.

Fig. 8. The portable LiDAR system is not only small, but it can also provide higher refreshing rate to meet the safety requirement in self-driving vehicles [8].

G. *Other Applications*

The technologies developed in LiDAR system have been deployed in a wide variety of applications. For example the architects use LiDAR to scan the buildings and historical sites for future maintenance. Lately the consumer electronics have applied such a pin-point capability into human machine interface (HMI), for example the Xbox from Microsoft, such that the users can communicate with computer intuitively. Moreover, the "Project Tango" proposed by Google integrate the LiDAR system with hand-held device [9]. With conventional CCD camera, infrared camera, and other censors, the depth map within tens of meters can be generated on a smart phone or a tablet.

III. Signal Processing and User Differentiation

A. *Parameter Extraction of the Overlapped Pulses*

As the adjacent targets get closer, the return laser pulses may be overlapped such that the estimation is incorrect or the pulses are taken as interference. To best approximate the received waveform, each pulse k is modeled as Gaussian distribution which include the mean μ_k, the standard deviation σ_k, and the magnitude A_k. The expectation and maximization (EM) algorithm can help to refine these parameters iteratively [10]. To differentiate the percentage of the pulse k in each sample i, the ratio $r_k^{(i)}$ is modeled as

$$r_k^{(i)} = \frac{\frac{A_k^{(i)}}{\sigma_k^{(i)}} \exp\left\{-\frac{1}{2}\left[\frac{x-\mu_k^{(i)}}{\sigma_k^{(i)}}\right]^2 + \min_k \frac{1}{2}\left[\frac{x-\mu_k^{(i)}}{\sigma_k^{(i)}}\right]^2\right\}}{\sum_{k=1}^{N} \frac{A_k^{(i)}}{\sigma_k^{(i)}} \exp\left\{-\frac{1}{2}\left[\frac{x-\mu_k^{(i)}}{\sigma_k^{(i)}}\right]^2 + \min_k \frac{1}{2}\left[\frac{x-\mu_k^{(i)}}{\sigma_k^{(i)}}\right]^2\right\}}. \quad (3)$$

After the ratio is derived, the pulses can be isolated and the corresponding parameters μ_k, σ_k, and A_k can be estimated as shown in Fig. 9. These parameters are applied in the next iteration for refinement. Eventually the estimation shall converge as the number of the iteration increases.

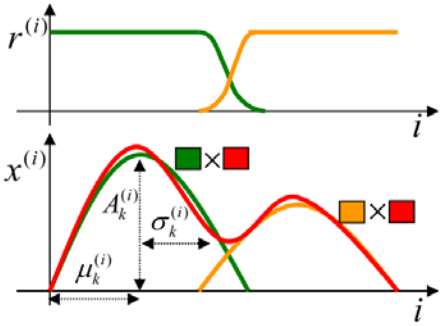

Fig. 9. Each pulse is approximated by Gaussian distribution, and the parameters of the overlapped pulses are estimated by iterative EM algorithm.

After the laser emitter triggers the detecting pulse, it shall wait for a period and start the next trigger. Therefore, the photodiode shall capture some long segments of background noise. Only the pulses which have abrupt rising and falling edges contain the valid samples for estimation. Without further information the channel quality is unknown and the magnitude of the channel noise may vary. Hence a dynamic threshold $\omega_{th}(i)$ at received sample i is required to separate the pulses from background noise

$$\omega_{th}(i) = \eta\left(\frac{1}{N}\sum_{j=i-w/2}^{i+w/2-1}|x(j)| - \frac{1}{N}\sum_{i-w/2}^{i+w/2-1}x(j)\right). \quad (4)$$

A sliding window with length w is defined as the period to be monitored. η is the coefficient for adjusting the dynamic range of the threshold. The channel noise is assumed to be Gaussian and the mean is expected to be 0. Therefore, the dynamic threshold in (4) becomes an envelope that is right above the noise. On the other hand, when a pulse signal is received, the

dynamic threshold in (4) shall be reduced to zero so that the pulse can surface from the background noise.

B. Encoded Pulses for User Differentiation

During the ranging, the estimation shall be compromised if the laser pulse is superimposed by other laser signal with the same wavelength. Both the ToF and the phase detection LiDAR are affected by such interference. If all the self-driving vehicles in the same filed use the same LiDAR system, it is likely that the LiDAR on the vehicle picks up the laser pulses or waves that are generated from other sources and performs erroneous estimation.

To differentiate the detecting signals from different LiDAR sources, it is recommended to encode or modulate the source signals so that each LiDAR device can discern its own signal. For example, the ToF LiDAR can use the pulse sequence that is generated by primitive polynomial. By rotating the sequence, the possibility that different LiDAR receivers pick up the same encoded sequence can be reduced. As to the LiDAR uses the phase difference for estimation, the symbols can be modulated as that are used in orthogonal frequency division multiplexing (OFDM). Since the transmitter and the receiver are both on the same platform, the timing and frequency offset can be well monitored. The applicable bandwidth is divided into multiple subcarriers, and different users can select different subcarrier combinations. Moreover, the selected subcarriers can be modulated with *M*-QAM. The estimation of the distance can therefore be acquired by computing the phase difference. With these methods, the user identity can be hidden in the encoded sequence or modulated symbols. Furthermore, the signal integrity can be preserved by DSP techniques such as tracking and equalization.

C. Rectification of Phases for Better Precision

The signal characteristics that are shown in time domain can also be interpreted in frequency domain. Therefore, the ratification in frequency domain can helps to process the signal in the time domain. The fast Fourier transform (FFT) convert the samples in time domain to frequency domain without losing generality. It is common to use the multiplications in frequency to replace the complex convolution in time domain. In addition the duality of FFT suggests that the time delay is the phase shift in frequency domain [11]

$$x[n-t_D] \leftrightarrow e^{-j\frac{2\pi}{N}kt_D} X[k] \,. \tag{5}$$

The timing acquisition using only convolution depends highly on the sampling rate of ADC. For example, if the sampling rate is 1GHz, the resolution of such ToF LiDAR shall be limited to 15cm. For better resolution the complexity in ADC design is higher. With the help of FFT and the duality in (5), such a limitation can be improved by comparing the phase difference between the modulated detecting symbols in the transmitter and the received symbols. The proposed architecture is as shown in Fig.10. As the laser emitter is triggered, the generated encoded sequence or symbol and the received signals are captured with the same amount of period. Due to the processing latency, a coarse timing synchronization using convolution and max value scan is applied to determine the start of the symbol. Afterwards the time domain samples are converted to the frequency domain symbols with *N*-FFT. At the receiver, the channel response and the imperfection in the photodiode and ADC devices cause additional interference to the received symbol. These offsets can be assessed by channel estimation. Therefore, the converted symbols are equalized by the coefficients that are provided from the channel estimation. The phases of the transmitted and the received symbols are tracked by coordinate rotation digital Computer (CORDIC) [12] subcarrier by subcarrier. For the subcarrier k, the phase difference is $e^{j\Delta_\theta[k]}$. With the duality in (5), the time delay of the k^{th} subcarrier is

$$t_D[k] = \frac{Nk}{2\pi}\Delta_\theta[k] \tag{6}$$

By averaging the delay, the distance is estimated as in (1).

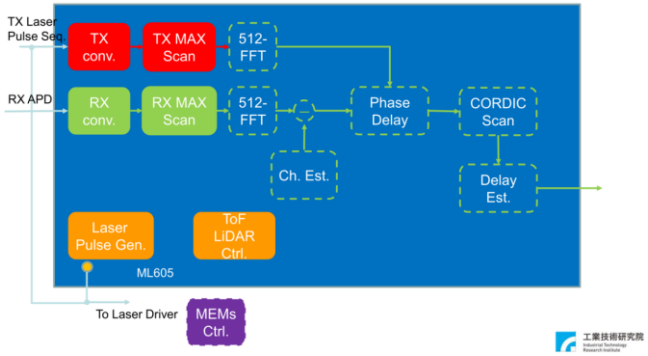

Fig. 10. The fundamental DSP blocks applied in multi-user LiDAR system.

IV. Simulation and Verification

A. Parameter Extraction of the Overlapped Pulses

The simulation results of the applied EM algorithm for extracting the overlapped pulses are as shown in Fig.11. First the received samples are smoothened by moving average to reduce the Gaussian noise. Afterwards the effective pulses are isolated by the dynamic threshold ω_{th} in (4). Finally, the three key parameters of Gaussian distribution are estimated through iterative EM algorithm. To verify the correctness, the pulses are reconstructed based on the estimated parameters as shown in red curves. In the simulation, the maximal number of overlapped pulses is set to four for implementation. Theoretically, the more the iteration, the better the estimation. To meet the real-time requirement, the number of iteration is set to three. According to the simulation results, the fix-point model is implemented on FPGA for prototyping.

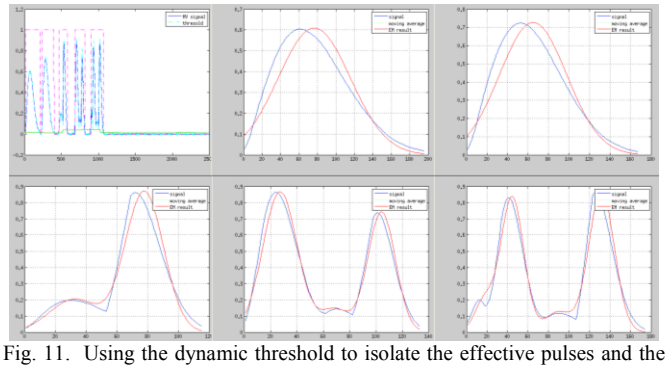
Fig. 11. Using the dynamic threshold to isolate the effective pulses and the EM algorithm to perform curve-fitting of the isolated pulses.

B. *Encoded Pulses and Rectification of Phases*

The proposed multi-user differentiation was implemented on FPGA platform as shown in Fig.12 for real-time depth map rendering. The encoded laser pulse was generated by Mitsubishi laser emitter which the wavelength was 658nm and the power was 100mW. The code sequence was modulated in FPGA. The 2D laser matrix was reflected by the MEMs mirror OP-6111 that was produced by OPUS Microsystems. As to the receiver, the avalanche photo diode (APD) C5658 that was produced by Hamamatsu was hooked to optical lenses for receiving the reflected laser pulses. The received power signal was sampled by the ADC and partially processed by the DSP function built in FPGA platform. Afterwards the processed raw data was fed back to PC and rendered by Matlab.

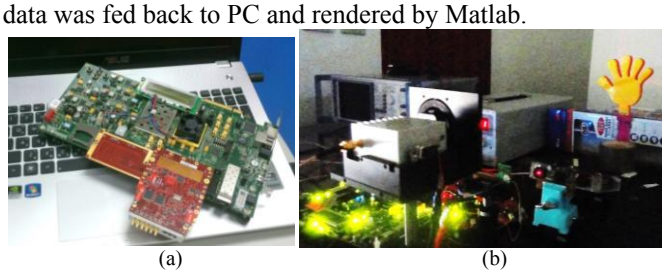

(a) (b)

Fig. 12. The hardware platform that is used to build the prototype: (a) Xilinx ML605 FPGA board with .4DSP FMC126 high speed ADC and conventional laptop installed with Matlab. (b) APD C5658 mounted with optical lens.

The ADC output of the received pulse sequence and the rendered result are as drawn in Fig. 13. Since the detecting laser pulses are encoded, the other laser sources with the same wavelength but different coding sequence did not affect the desired inputs to the receiver. Hence, the proposed system is robust against different LiDAR devices. For fast prototyping, the DSP blocks such as FFT and the phase offset estimation were implemented in Matlab for better flexibility. Therefore, the bottleneck of the throughput was at these blocks. The update of the depth map was one frame per second with resolution 256 by 256. If the entire DSP blocks are implemented on FPGA, which means only the depths and the 2D coordinates were the only payloads to software, it is estimated that the throughput of updating can be increased at least by 10 times.

Let us discuss the accuracy of the estimation with the proposed algorithm. The tests were performed with and without ambient light which are annotated as ‘Amb’ and ‘Dark’, and the distance estimations were performed with only convolution and with additional phase rectification which are annotated as ‘Conv’ and ‘Phase’. Each type of the tests were performed 10 times and the mean and the standard deviation are presented. In Fig. 13, the horizontal unit is 2.5cm and the vertical unit is 12cm. There is an estimation offset due to the internal delay in the hardware platform. For the tests with only convolution, the mean of the estimations is 12cm more on average than that with additional phase rectification as shown in Fig.13(a). Moreover, the standard deviation in the estimation using only convolution is more erratic as shown in Fig.14. The estimation with additional phase rectification provides more consistent results.

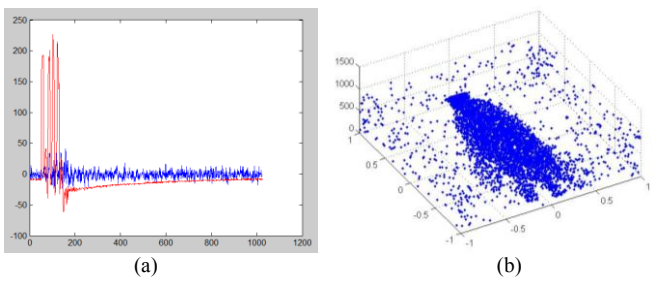

(a) (b)

Fig. 13. (a) The transmitted (red) and the received (blue) encoded laser pulse sequence (b) The detected hand toy that was placed 50cm in front of the laser gun and captured by the proposed prototype.

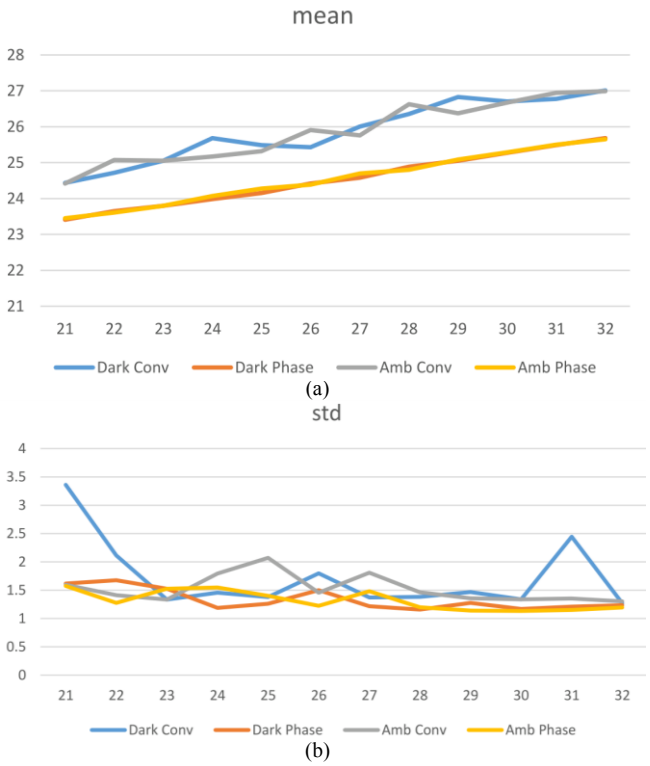

Fig. 14. (a) The transmitted (red) and the received (blue) encoded laser pulse sequence (b) The detected hand toy that was placed 50cm in front of the laser gun and captured by the proposed prototype.

V. Conclusion and Future Works

The targets of this work focus on parameters extraction of the overlapped laser pulses using iterative EM algorithm. Additionally the encoded pulse sequences are applied to differentiate the LiDAR users in the same field, and the phase rectification helps to refine the distance estimation, such that the precision of the 3D depth map can be improved. Due to the inadequacy of the optical lens, the viewable range was not wide enough to generate more abundant detection. However, the tests over the hardware platform have proven that the proposed algorithm helps counteract the imperfection in the optical channels, and the estimations are converged accordingly. Moreover, the proposed method, which uses encoded pulse sequence, is suitable for multiple LiDAR systems function in the same filed at the same time. Further signal processing techniques such as timing and frequency tracking that are used in OFDM architecture shall be applied in the future study. To better counteract the channel imperfection and the variation in different devices, we will add in the gain control and adaptive filter to excavate the received samples that are buried in the background noise. In this work the DSP approach for signal

capture, equalization, and reconstruction has been effectively proven. The next step is to use the off-the-shelf devices for the portable LiDAR system which can be installed on self-driving car.

REFERENCES

[1] (2014) The website [Online] Available: http://www.4erevolution.com/en/affordable-autonomous-car/

[2] J. Kostamovaara, K. Maatta, and R. Myllyla,"Pulsed time-of-fight laser rangefinding techniques for industrial applications," in *Proc. SPIE Conf. Intelligent Robotic Systems-Optics, Illumination and Image Sensing for Machine Vision*, Nov. 1991, vol. 1614, pp. 283-295.

[3]"LIDAR 與環境調查 / 監測 / 災害防救應用" 國土資訊系統通訊 2007.03 徐偉城

[4] Ou-Yang, M., Huang, C.-Y., Chen, J., "High-dynamic-range laser range finders based on a novel multimodulated frequency method," (2006) *Optical Engineering*, 45 (12), art. no. 123603.

[5] (2014) The website [Online] Available: http://www.opusmicro.com.tw/

[6] D. Mongus and B. Zalik, " Computationally efficient method for thegeneration of a digital terrain model from airborne LiDAR data using connected operators, " *IEEE J. Sel. Topics Appl. Earth Observ.*, vol. 7, no. 1, pp. 340-351, Jan, 2014

[7] K. Ito, C. Niclass, I. Aoyagi, H. Matsubara, M. Soga, S. Kato, M. Maeda, and M. Kagami, "System design and performance characterization of a MEMS-based laser scanning time-of-flight sensor basedon a 256 64-pixel single-photon imager," *IEEE Photon. J.*, vol. 5,no. 2, 2013

[8] A 0.18-µm CMOS SoC for a 100-m-Range 10-Frame/s 200 96-Pixel Time-of-Flight Depth Sensor (2014)

[9] (2014) The website [Online] Available: https://www.google.com/atap/project-tango/

[10] Leite, J.A.F.; Hancock, E.R., "Iterative spline relaxation with the EM algorithm," Pattern Recognition, 1996., *Proceedings of the 13th International Conference on* , vol.2, no., pp.161,165 vol.2, 25-29 Aug 1996

[11] A. V. Oppenheim and R. W. Schafer, Discrete-Time Signal Processing, 3rd ed., *Prentice Hall*, 2009.

[12] Hu, Y.H., "CORDIC-based VLSI architectures for digital signal processing," *Signal Processing Magazine, IEEE* , vol.9, no.3, pp.16,35, July 1992

Kai-Jiun Yang received his M.S. Degree in electrical engineering from University of Southern California, USA, in 2001. His research interests include VLSI design and verification, DSP, communication system, and the theory in estimation. Currently he is with the System Integration & Applications Department, Division for Embedded System & SoC Technology, ICL. He is also working toward the Ph.D. degree in electrical and control engineering from the National Chiao-Tung University. E-mail: ykj@itri.org.tw

Chi-Tien Sun received his M.S. degree in electronic and information engineering from Yuan-Ze University, Taiwan, in 1994. His primary research areas were communication system, DSP and digital IC design. He is now the manager of the System Integration & Applications Department, Division for Embedded System & SoC Technology, ICL, ITRI. E-mail: ctsun@itri.org.tw.